SPECTRAL ANOMALY DETECTION FOR THE MAPPING AND IMAGING SPECTROMETER FOR EUROPA (MISE). Kiri L. Wagstaff[1], Diana L. Blaney[1], Srija Chakraborty[1,2], Steve Chien[1], Ashley Davies[1], Serina Diniega[1], and Gary Doran[1], [1]Jet Propulsion Laboratory, California Institute of Technology, 4800 Oak Grove Drive, Pasadena, CA, 91109-8099, USA (kiri.wagstaff@jpl.caltech.edu), [2]Arizona State University.

Introduction: The *Europa Clipper* mission [1], scheduled to launch in 2023, will conduct 40+ flybys of Jupiter's moon Europa and collect observations using nine instruments. Each flyby is likely to reveal new discoveries about Europa that will increase our understanding of the subsurface ocean and influence future mission plans. Due to the distance between Europa and Earth, *Clipper* will be downlink-limited: the instruments have the ability to collect more data than can be transmitted. Traditional mission planning operations will tailor each flyby's data collection activities to fit the available resources (time, power, and downlink). We are exploring software advances that would enable *Clipper* to collect additional data, analyze it onboard to assign downlink priorities, and potentially increase science return without increasing downlink consumption.

Spacecraft onboard data analysis: Several missions now can analyze data *in situ* and make decisions about downlink priorities and follow-up observations. The EO-1 spacecraft in Earth orbit analyzed hyperspectral data from the Hyperion instrument to detect floods and volcanic eruptions [2], detect surface sulfur deposits (a potential Europa analog biosignature) [3], and assess image quality in terms of cloud cover to optimize downlink [4]. The IPEX CubeSat, also in Earth orbit, used machine learning to generate image classification maps as low-bandwidth summary products and detect regions of high visual interest for priority downlink [5]. The Mars Science Laboratory rover uses onboard image analysis to select targets in Navcam images and collect new observations of those targets autonomously with the ChemCam laser spectrometer [6].

Clipper has several instruments that can potentially benefit from onboard analysis as the data is collected. We developed a method for detecting thermal anomalies (hot spots) in data collected by the E-THEMIS thermal imager [7]. Hot spots could indicate subsurface upwelling or processes related to plume activity. In this work, we focus on analysis of data collected by the MISE imaging spectrometer [8], which generates a much higher data volume and therefore could benefit even more from onboard analysis and prioritization of data.

Spectral anomaly detection: There are specific minerals (e.g., hydrated salts and sulfates) that are already known to be of potential interest on Europa. Specific pattern matching detectors can be employed to detect and prioritize those observations within MISE data. Yet in all missions designed for the exploration of new environments and worlds, there is value in also detecting the unexpected. We employ anomaly detection methods to identify surface areas with unusual composition.

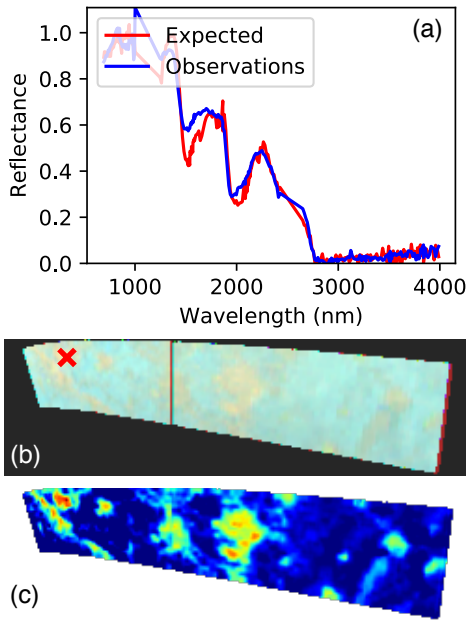

Figure 1: Spectral anomaly found in *Galileo* NIMS data set 14e006ci.qub using the DEMUD algorithm. (a) Explanation for why this pixel was considered anomalous, (b) Spatial plot with anomalous pixel marked with red x, (c) Abundance plot showing locations of similar pixels.

We explored two anomaly detection methods. The Reed-Xiaoli (RX) method [9] assigns an anomaly score A to each pixel x that captures its deviation from the "background" or typical signals in the data set:

$$A_{RX}(x) = (x - \mu)^T \Sigma^{-1} (x - \mu), \quad (1)$$

where μ is the mean across all pixels and Σ is the covariance matrix. The DEMUD method [10] iteratively models pixels as they are selected using the top k components of a Singular Value Decomposition (SVD) of the pixels and assigns an anomaly score to the remaining pixels based on their reconstruction error:

$$A_D(x) = ||x - (UU^T(x - \mu) + \mu)||_2, \quad (2)$$

where U contains the k principal components and $UU^T(x - \mu) + \mu$ is the reconstruction of x using U.

DEMUD is unique amongst anomaly detection methods in that it also provides an explanation for its selections

by highlighting which features cause the greatest reconstruction error (i.e., which feature values could not be well modeled by previous observations). For example, it has been used to detect and explain unusual mineralogy in MSL ChemCam observations [11].

Results with NIMS data: *Galileo* NIMS provides an analogue for the MISE instrument. NIMS observed Europa (and other targets) at $0.7 - 5.2$ μm, versus $0.8 - 5.0$ μm for MISE. Figure 1 shows example output of the DEMUD algorithm when applied to a NIMS observation of Europa. DEMUD selected the pixel corresponding to the red x in Figure 1(b) and plotted the model's prediction (red) and actual data (blue) in Figure 1(a). Wavelengths where the two spectra diverge are diagnostic for this pixel. Figure 1(c) shows an abundance plot with a heatmap in which red areas are similar to the selected pixel and blue areas are dissimilar. This component within the data set occurs in several areas; it is an anomaly only the first time it is encountered by the algorithm. As DEMUD iterates, it also finds and flags data with quality issues, such as the vertical stripe to the left of the middle of the region. Careful review of each detected "outlier" enables the determination of whether it is of scientific interest or an artifact. We are currently expanding our analysis to include a larger collection of NIMS Europa observations, which could lead to new insights into this data set that can inform mission planning for *Clipper*.

We also conducted controlled sensitivity experiments in which we artificially perturbed a randomly selected NIMS pixel and evaluated whether the modified pixel was detected. We perturbed the pixel by linearly mixing it with the spectrum s for a mineral of interest from the USGS NIMS spectral library [12], which covers $0.2 - 3.0$ μm: $x' = fs + (1 - f)x$, where f is the anomaly fraction. Figure 2 shows the novelty detection rank (i.e., speed with which a given perturbed pixel is discovered), for NIMS data set 14e002ci.qub. Discoverability increases as the perturbed pixel is more anomalous. A supervised method that is trained to detect the mineral of interest ("MF" stands for "matched filter") provides an upper bound on anomaly-based discoverability. We found that RX and DEMUD detected the perturbed pixels at about the same rate (e.g., within $10 - 50$ selections for an anomaly fraction of 0.5). These results provide information about how easy or difficult it would be to detect a given mineral on Europa (e.g., bloedite is easier to detect than epsomite); discoverability varies since some minerals are inherently more similar or different to Europa's composition.

Discussion: Our ground-based experiments with NIMS observations of Europa provide a proof of concept for spectral anomaly detection methods that could be employed for the autonomous analysis of MISE data. This analysis could be done onboard the spacecraft to help prioritize data for downlink (e.g., observations with a high anomaly score could receive high priorities, or regions around an anomaly could be cropped to generate a smaller product that focuses on an area of high interest). It could also be used on the ground to direct attention to small areas with anomalous composition that merit deeper investigation.

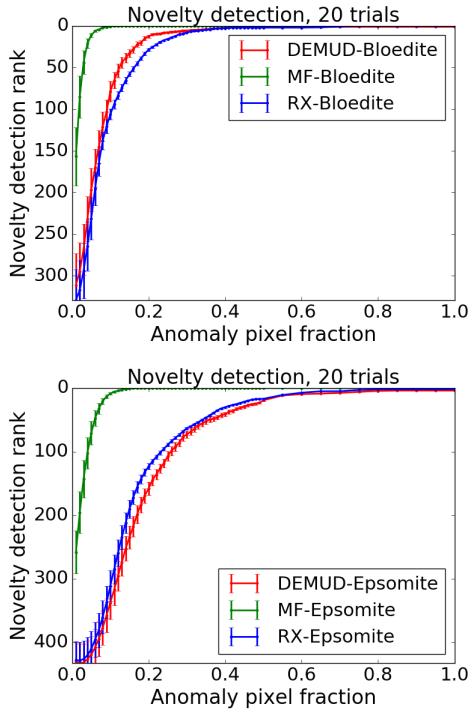

Figure 2: Discoverability for artificially perturbed pixels in *Galileo* NIMS data set 14e002ci.qub. The perturbed pixel was mixed with library spectra for bloedite (top) or epsomite (bottom). "MF" stands for a matched filter trained to detect the specified mineral.

References: [1] Pappalardo, R.T. *et al.* (2017) *EPSC*. [2] Chien, S. *et al.* (2005) *J. Aerospace Computing, Info., and Comm.*. [3] Mandrake, L. *et al.* (2012) *ACM Trans. on Intelligent Sys. and Tech.* [4] Wagstaff, K.L. *et al.* (2017) *IJCAI Workshop on AI in the Oceans and Space*. [5] Chien, S. *et al.* (2017) *J. Aerospace Info. Sys.* [6] Francis, R. *et al.* (2017) *Science Robotics*. [7] Doran, G. *et al.* (2018) *EPSC*, Abstract #1248. [8] Blaney, D. *et al.* (2017) *LPSC*. [9] Reed, I.S. and Yu, X. (1990) *IEEE Trans. Acoustic Speech and Signal Proc.* [10] Wagstaff, K.L. *et al.* (2013) *AAAI*. [11] Wagstaff, K.L. *et al.* (2014) *LPSC*. [12] Clark, R.N. *et al.* (1993) *USGS* report 93-592.

Acknowledgments: This work was carried out at the Jet Propulsion Laboratory, California Institute of Technology, under a contract with the National Aeronautics and Space Administration. Government sponsorship acknowledged. © 2019, California Institute of Technology.